ACS Sustainable Chemistry & Engineering

Research Article

pubs.acs.org/journal/ascecg

Plant-Mediated Synthesis of Ag–Pd Alloy Nanoparticles and Their Application as Catalyst toward Selective Hydrogenation

Fenfen Lu,[†] Daohua Sun,*[,†] Jiale Huang,[†] Mingming Du,[†] Feng Yang,[†] Huimei Chen,[†] Yingling Hong,[†] and Qingbiao Li*[,†,‡]

[†]Department of Chemical and Biochemical Engineering, College of Chemistry and Chemical Engineering, Fujian Provincial Key Laboratory of Chemical Biology, Xiamen University, Xiamen, 361005, P.R. China

[‡]College of Chemistry & Life Science, Quanzhou Normal University, Quanzhou, 362002, P.R .China

ABSTRACT: Herein, we reported the green synthesis of Ag–Pd alloy nanoparticles (NPs) using the aqueous extract of the *Cacumen platycladi* leaves as well as their application as catalyst for hydrogenation of 1,3-butadiene. The biosynthetic NPs were characterized to confirm the nature of alloy by UV–vis spectroscopy, X-ray diffraction (XRD), transmission electron microscopy (TEM), and energy dispersive X-ray spectroscopy (EDX). The possible functional groups responsible for the reduction and protection of NPs were identified through Fourier transform infrared spectroscopy (FTIR). The results revealed that biomolecules like saccharides, polyphenols, or carbonyl compounds were related to the reduction process, and the (NH)C=O groups were responsible for the stabilization of the NPs. Furthermore, the as-formed Ag–Pd bimetallic-supported catalysts especially $Ag_1Pd_3/\gamma\text{-}Al_2O_3$ was found to possess excellent catalytic performance toward hydrogenation of 1,3-butadiene. A butene yield of 84.9% was obtained, which was remarkably enhanced when compared with monometallic counterparts. Moreover, the activity of it maintained stability within 12 h of durable experiments.

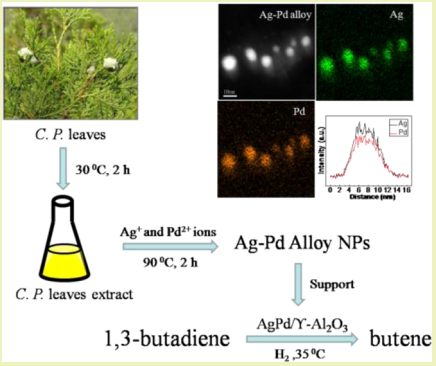

KEYWORDS: *Biosynthesis, Ag–Pd Nanoparticles, Alloy, Cacumen platycladi*

INTRODUCTION

Bimetallic nanoparticles (NPs) with alloy or core–shell structures have received special attention over recent years due to their possible applications in catalysis, electronics, optical, coatings, and medical science.[1−7] Bimetallic alloy NPs have been synthesized in different ways such as in gas phase, in solution, or being supported onto a solid substrate matrix.[8] Among them, the most common approach is the chemical reduction method, in which the metal precursor is reduced by a reducing agent (e.g., $NaBH_4$ or H_2) in the presence of stabilizer molecules (e.g., PVP, PVA, or sodium citrate) in an appropriate solvent.[9−13] Though chemical reduction methods in the literature have successfully achieved bimetallic NPs with desired sizes and shapes, the processes often involve chemical reagents that are nonbiodegradable or detrimental to the environment.[14,15] Hence, the development of nontoxic, environmentally benign, and inexpensive procedures to synthesize bimetallic alloy nanomaterials is important. Accordingly, a biological approach that utilizes the "nature factory" (namely, plants and microorganisms) has emerged as a novel method for the synthesis of various metal nanostructures. Compared with the elaborate process of maintaining cell cultures, plants are inexpensive and easily available, and their aqueous extracts are rich in reducing biocompounds such as polyols as well as surface-stabilizing components such as proteins. Therefore, in recent years, a long list of plant species were employed for successful formation of various kinds of metal NPs. For instance, Ag or Pd NPs has been synthesized using the leaf/seed extract of *Pedilanthus tithymaloides*,[16] *Catharanthus roseus*,[17] *Coleus aromaticus*,[18] *Vitex negundo* L.,[19] alfalfa sprouts,[20] *Cinnamomum camphora*,[21] *Solanum trilobatum*,[22] coffee, and tea.[23] Existing research on biosynthesis of monometallic NPs was extensive; nonetheless, the research on biosynthesis of bimetallic NPs was seldom reported so far, except for a few attempts on Au/Ag,[14,24−26] Ti/Ni,[27,28] and Au/Pd.[24]

In earlier studies, our research groups obtained Ag and Pd monometallic NPs using different plant extracts in aqueous solutions.[21,29−32] In this paper, we report a facile and green synthesis of Ag–Pd alloy bimetallic NPs using *Cacumen platycladi* leaves extract as the source of both reductant and stabilizer. To the best of our knowledge, this is the first report about plant-mediated formation of Ag–Pd alloy bimetallic NPs. The process involves the simultaneous bioreduction of $AgNO_3$ and $Pd(NO_3)_2$ using the extract at 90 °C without addition of any other surfactants. The possible functional groups responsible for the reduction and protection of the as-formed NPs were monitored with Fourier transform infrared spectroscopy (FTIR), while the alloy nature of the bimetallic NPs were characterized using various characterization techniques includ-

Received: January 20, 2014
Revised: March 5, 2014
Published: April 1, 2014

ing UV−vis spectroscopy, X-ray diffraction (XRD), transmission electron microscopy (TEM), selected area electron diffraction (SAED), and energy dispersive X-ray spectroscopy (EDX). Also, supported Ag−Pd bimetallic catalysts were prepared from the as-formed bimetallic NPs, and they demonstrated high catalytic activity toward 1,3-butadiene hydrogenation.

EXPERIMENTAL SECTION

Chemicals and Materials. Sundried *Cacumen platycladi* leaves were purchased from Xiamen Jiuding Drugstore (China). Silver nitrate ($AgNO_3$) was purchased from Sinopharm Chemical Reagent Co., Ltd. (China). Palladium nitrate ($Pd(NO_3)_2$) was purchased from Aladdin Reagent Co., Ltd. (China) and used as received.

Synthesis of Ag−Pd Alloy NPs. The *Cacumen platycladi* leaves were milled, and 1.0 g of the milled powder was dispersed into a 250 mL conical flask with 100 mL of deionized water and kept in a water bath shaker at 30 °C. After 2 h, the mixture was filtered to obtain the extract. To synthesis bimetallic Ag−Pd NPs, 10 mL of an aqueous solution mixture of $AgNO_3$ and $Pd(NO_3)_2$ (0.5 mM of the concentration of total metal) was heated to 90 °C in a oil bath with a constant temperature and a stirring rate of 600 rpm. Subsequently, 10 mL of the *Cacumen platycladi* leaves extract was added to this precursor solution with vigorous stirring for 2 h, and the end products were obtained accordingly. The composition of Ag−Pd NPs could be controlled by changing the ratio of the metal precursor ($AgNO_3$/$Pd(NO_3)_2$ ratios were 3:1, 1:1, 1:3). For comparison, the monometallic NPs were prepared in the same manner by substituting a mixture of $AgNO_3$/$Pd(NO_3)_2$ solution with $AgNO_3$ (0.5 mM) or $Pd(NO_3)_2$ (0.5 mM) solutions.

Characterization of Ag−Pd Alloy NPs. UV−vis spectroscopic analyses of Ag−Pd alloy NPs were carried out as a function of bioreduction time at room temperature using a UV-1800 spectrophotometer (Shimadzu, Japan) at a resolution of 1 nm. The dried and powdered samples were then analyzed via XRD using an X-ray diffractometer (Phillips, Netherlands) with Cu Kα radiation (40 kV, 30 mA). Samples for TEM were prepared by placing a drop of as-prepared hydrosol on carbon-coated copper grids and allowing water to completely evaporate. TEM samples were observed on a Tecnai F30 Microscope (FEI, The Netherlands). In order to identify the biomolecules responsible for the formation of bimetallic NPs in *Cacumen platycladi* leaves extract, FTIR experiments were carried out. In a typical process, the extract before reaction and the resulting solutions after biosynthesis of NPs was dried at 50 °C. Then, the dried samples were ground with KBr (dried at 120 °C) and analyzed by a Nicolet 6700 spectrophotometer (Thermo Nicolet, U.S.A.).

Preparation of Ag−Pd/γ-Al_2O_3 Catalysts and Catalytic Hydrogenation Reactions. The monometallic and bimetallic sol were prepared according to procedures mentioned in the above section. To prepare the supported catalyst, the weighed amount of γ-Al_2O_3 support was added into the as-formed hydrosol (to keep the metal concentration 0.5 wt %), and HCl was also added to maintain the pH value at around 2. After the mixture was stirred vigorously for another 1 h, the suspension was filtered through a cellulose filter membrane with a pore size of 0.8 mm. The filter residue was washed three times with deionized water and finally dried in a vacuum oven at 50 °C for 12 h. Bimetallic catalysts with different Ag/Pd molar ratios were prepared. Specifically, the $AgNO_3$/$Pd(NO_3)_2$ ratios were 3:1, 1:1, 1:3, and the responding catalysts were labeled as Ag_3Pd_1/γ-Al_2O_3, Ag_1Pd_1/γ-Al_2O_3, and Ag_1Pd_3/γ-Al_2O_3, respectively. For instance, Ag_1Pd_1/γ-Al_2O_3 corresponds to the γ-Al_2O_3-supported catalyst with an initial Ag/Pd molar ratio of 1:1.

The hydrogenation of 1,3-butadiene was carried out at 35 °C in a fixed bed flow stainless reactor (i.d. Six mm) under atmospheric pressure. The temperature was measured by a glass tube-covered Cr−Al thermocouple located in the center of the catalyst bed. Before the reaction, 50 mg of catalyst was loaded into the reactor; the feed contained 2.15% 1,3-butadiene, 4.30% H_2, and N_2 as balance gas, and flow rate was adjusted to 13.5 mL min^{-1} with mass flow meter (Sevenstar Electronics). The reactor effluent was analyzed on line every 20 min using a gas chromatograph (GC) equipped with an Al_2O_3 column and a FID detector. The conversion and selectivity were determined from the areas of GC peaks corresponding to the reactant (1,3-butadiene), main products (1-butene, *cis*-2-butene and *trans*-2-butene), and side product (butane).

RESULT AND DISCUSSION

UV−Vis Spectra and XRD Analysis. The formation of NPs was primarily characterized by UV−vis spectroscopy, which has been extensively used in synthesis of NPs with surface plasmon resonance (SPR) bands.[33,34] Figure 1 shows

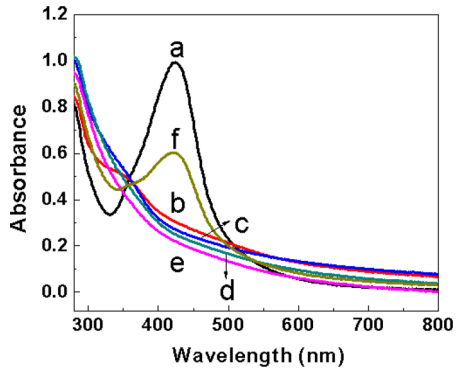

Figure 1. UV−vis spectra of monometallic nanoparticles AgNPs (a), PdNPs (e), physical mixture of Ag and Pd NPs (1:1/v/v) (f), and Ag−Pd bimetallic nanoparticles with an initial Ag/Pd molar ratio of 3:1 (b), 1:1 (c), and 1:3 (d).

UV−vis absorbance behavior of the both the biosynthesized monometallic and bimetallic NPs. As observed in Figure 1e, the monometallic AgNPs exhibited characteristic SPR bands centered at 426 nm, and no peak was present for the monometallic PdNPs from 300 to 800 nm, which was consistent with previous reports.[35−37] The direct physical mixture (1:1/v/v) sample of monometallic AgNPs and PdNPs has little effect on the SPR band of AgNPs (Figure 1f). Nonetheless, for the as-formed bimetallic Ag−Pd NPs, the featured SPR band of the AgNPs completely disappeared in all of the samples prepared at different initial Ag/Pd molar ratios. Such a difference in the UV−vis spectra suggested that the nanoproduct may be alloy rather than a physical mixture of AgNPs and PdNPs.[35,38]

XRD patterns in Figure 2 further confirmed the bimetallic nature of the co-bioreduction products synthesized with different initial Ag/Pd molar ratios. As shown, an intense peak of Ag−Pd bimetallic NPs were found at 38.9° (2θ), 39.3°, and 39.6° for the samples prepared at the initial Ag/Pd molar ratio of 3:1, 1:1, 1:3, respectively. All of these peaks located between the values of pure Ag crystal (111) at 37.9° (ref. code: 00-001-1164) and pure Pd crystal at 40.0° (ref. code: 00-046-1043), and the location of the peak shifted closer toward that of the pure Pd crystal with the increasing Pd fraction. Such results further verified the alloy structure of the as-synthesized NPs.

TEM and SAED Analysis. Figure 3 shows the TEM images of the bimetallic NPs and monometallic NPs. The size of the monometallic AgNPs is 22.0 ± 4.5 nm, and the size of the PdNPs is 7.3 ± 0.4 nm (Figure 3A and E). The sizes of the bimetallic NPs with initial Ag/Pd molar ratios of 3:1, 1:1, and 1:3 were 11.9 ± 0.8, 9.1 ± 0.7, and 7.4 ± 0.4 nm (Figure 3B, C, and D), respectively. Figure 3F plots the average particle size of

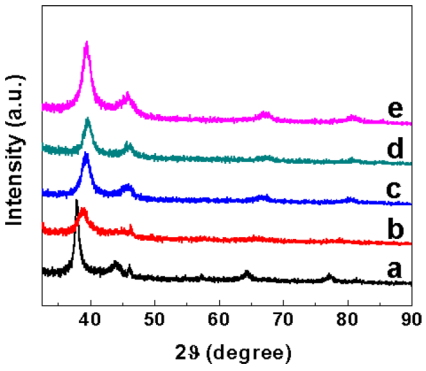

Figure 2. XRD patterns of monometallic nanoparticles AgNPs (a), PdNPs (e), and Ag–Pd bimetallic nanoparticles with an initial Ag/Pd molar ratio of 3:1 (b), 1:1 (c), and 1:3 (d).

the bimetallic and monometallic NPs versus the Pd molar fractions. Evidently, the average particle size of as-synthesized NPs decreased with increasing palladium content. The influence of the metal molar ratio on the size of the alloy bimetallic NPs has also been reported in earlier studies.[39,40] The dependence of the size of the alloy NPs on the different compositions relates to the collision energy, sticking coefficient, rates of nucleation, and growth. High-resolution TEM (HRTEM) allows for direct imaging of the atomic structure of the bimetallic NPs. Figure 4A manifests that the lattice spacing of the as-synthesized bimetallic NPs is 2.28 Å, which is between that of individual AgNPs (2.36 Å) and PdNPs (2.25 Å). The SAED pattern of the Ag–Pd bimetallic NPs showed five diffraction rings (Figure 4B), which indicated five intense

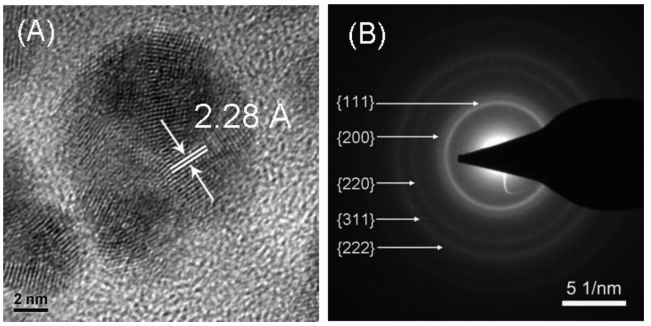

Figure 4. High-resolution TEM (HRTEM) image (A) and small-area electrodiffraction (SAED) patterns (B) of the as-biosynthesized Ag–Pd alloy nanoparticles with an initial molar ratio of 1:1.

peaks of (111), (200), (220), (311), and (222) in the face-centered cubic crystal structure.

EDX Elemental Analysis. In order to investigate the Ag and Pd element distribution of the bimetallic NPs, scanning TEM (STEM)-EDX mapping images are shown in Figures 5 and 6. These colored elemental mapping images prove that regardless of the initial mole ratio of Ag/Pd, the Ag (green, Figure 5B, E, and H) and Pd (orange, Figure 5C, F, and I) were homogeneously distributed over the entire NPs. EDX elemental line scanning on a single particle (Figure 6) also confirmed that the as-synthesized NPs were alloyed in essence.

FTIR Analysis. FTIR analysis was employed to identify the possible functional groups responsible for the bioreduction of the metal precursors and the stabilization of the NPs[31,32] in *Cacumen platycladi* leaves extract. The peaks at 3430, 2930, 1612, 1510, 1387, 1272, and 1056 cm^{-1} are observed (Figure

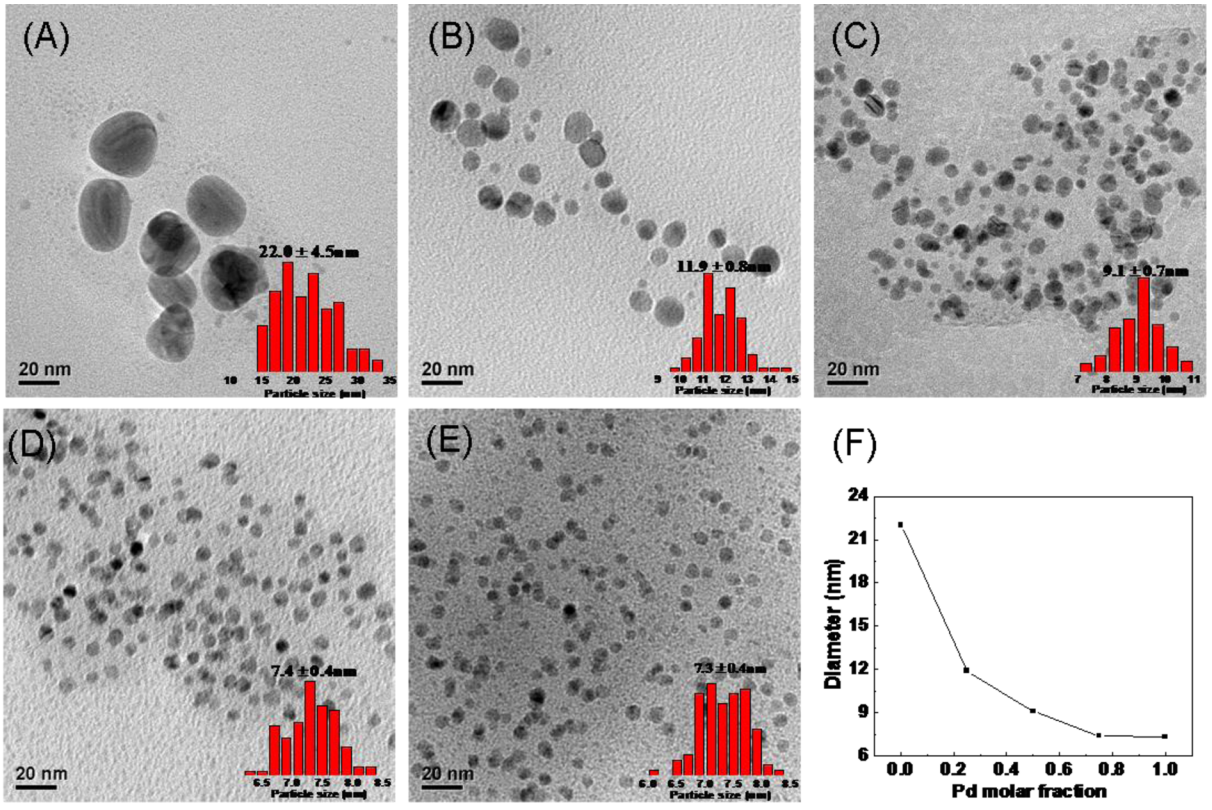

Figure 3. TEM images and size histograms (inlet) of biosynthesized Ag–Pd bimetallic nanoparticles with initial Ag/Pd molar ratios of (B) 3:1, (C) 1:1, and (D) 1:3; monometallic nanoparticles (A) AgNPs and (E) PdNPs; and (F) plot of the average particle size vs Pd molar fraction.

dx.doi.org/10.1021/sc500034r | *ACS Sustainable Chem. Eng.* 2014, 2, 1212–1218

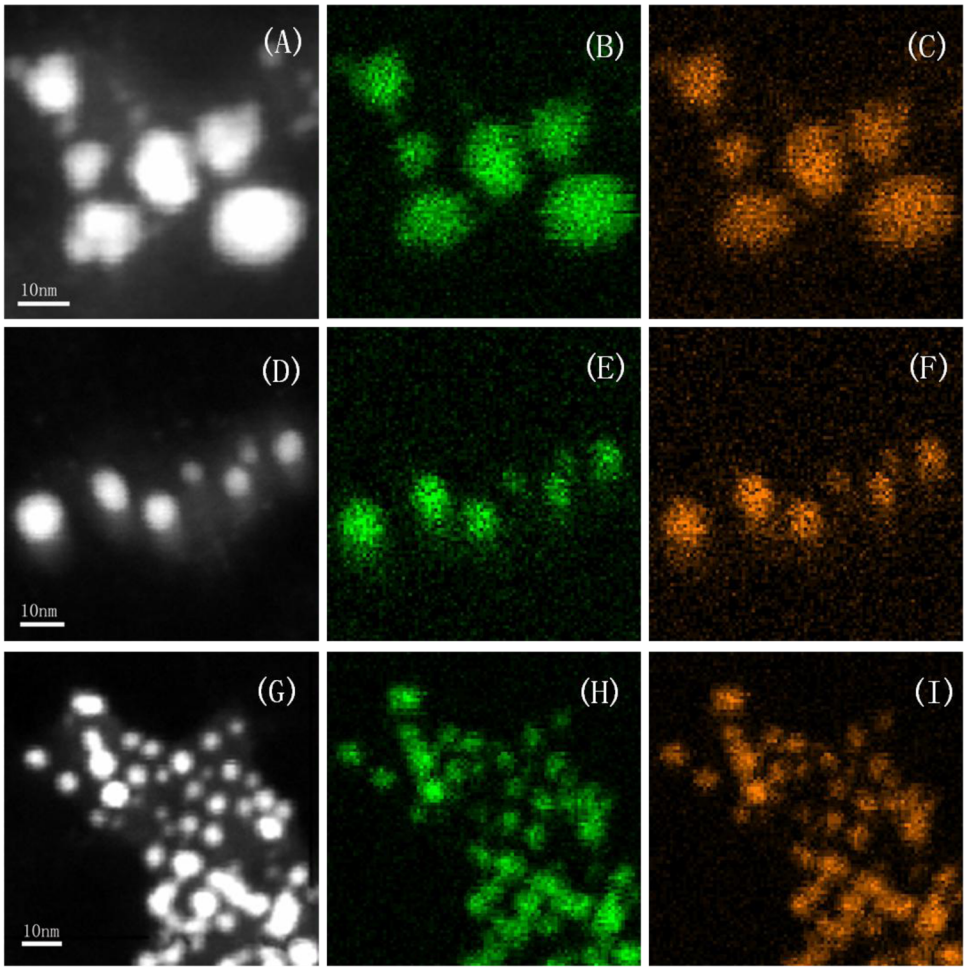

Figure 5. STEM images of the Ag−Pd bimetallic nanoparticles with initial Ag/Pd molar ratios of (A) 3:1, (D) 1:1, and (G) 1:3; EDX elemental maps of Ag (B, E, and H) and Pd (C, F, and I) concentrations in the alloy nanoparticles.

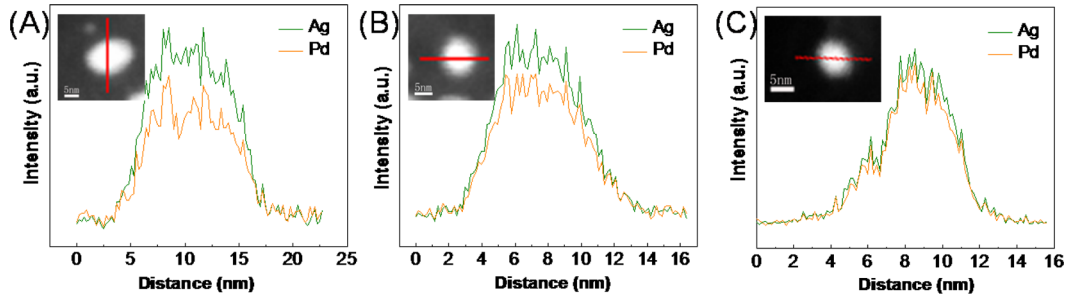

Figure 6. Distributions of Ag and Pd components along the cross-sectional compositional line profiles of a single Ag−Pd nanoparticle with initial Ag/Pd molar ratios of (A) 3:1, (B) 1:1, and (C) 1:3.

7b) before bioreduction. Generally, the peaks at 1056 and 1272 cm^{-1} are attributed to the hydroxyl in carbohydrate and the C−O stretching vibration in cyclic compounds, respectively. The peaks at 1384 and 2930 cm^{-1} may be ascribed to the bending vibration and stretching vibration of C−H in alkanes. The peak at 1510 cm^{-1} was referred to C═C in aromatic compounds. The peaks at 1612 cm^{-1} belonged to the (NH)C═O groups, and the peaks at 3430 cm^{-1} were assigned to the O−H stretching vibration in alcohols and phenolic compounds, respectively. Therefore, we concluded that the possible biomolecules in the *Cacumen platycladi* leaves extract may include saccharides, polyphenols, protein, and carbonyl compounds.

The FTIR spectra of *Cacumen platycladi* leaves extract after reacting with $AgNO_3$ and $Pd(NO_3)_2$ for 2 h at 90 °C is present in Figure 7c and that of the as-biosynthesized alloy NPs after being washed three times is shown in Figure 7a. Comparison between Figure 7b and c revealed that the intensity of peaks at 1056, 1272, and 2930 cm^{-1} decreased after the biosynthetic reaction, which manifested that the reaction involved several compounds such as carbohydrate, cyclic, and alkanes. Besides, the peak at 1612 cm^{-1} in Figure 7b shifted to 1632 cm^{-1} in both the extract residues left after the reaction as well as in the as-formed products. Such a result was attributed to the binding of the (NH)C═O groups with the as-synthesized NPs.[24] Earlier studies have demonstrated that the C═O group could

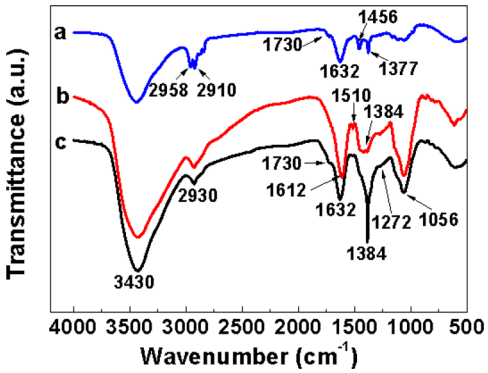

Figure 7. FTIR spectra of Ag−Pd alloy nanoparticles (a), *Cacumen platycladi* leaves extract before bioreduction (b), and *Cacumen platycladi* leaves extract after bioreduction (c).

coordinate with the PdNPs surface and therefore stabilize the particles.[41] New peaks at 1730 cm^{-1} (Figure 7c and a) and 1456 cm^{-1} (Figure 7a) appeared, which could owe to the C═O stretching vibration in carbonyl compounds and the C═C in aromatic compounds, respectively. On the basis of the above FTIR analysis, we speculate the saccharides or carbonyl compounds are responsible for the reduction of aqueous metal precursors, and the biocompounds with the (NH)C═O groups such as proteins are related to the stabilization of the NPs.

Catalytic Activity Evaluation. The Pd catalyst is mostly used in the selective hydrogenation of 1,3-butadiene as 1,3-butadiene exhibits stronger adsorption on the Pd surface than butane.[42,43] Addition of other metals to the Pd catalyst is an efficient way to improve the butane selectivity by modifying the structural and electronic properties of Pd.[44,45] Here, as-biosynthesized Ag, Pd monometallic NPs, and Ag−Pd alloy bimetallic NPs with different initial Ag/Pd ratios supported on γ-Al_2O_3 were used for selective 1,3-butadiene hydrogenation. As shown in Table 1, Ag/γ-Al_2O_3 is completely inactive in 1,3-butadiene hydrogenation. With increasing Pd contents, the conversion of the 1,3-butadiene increases monodirectionally. This confirmed that Pd was the active component for this hydrogenation reaction. The bimetallic catalysts Ag_3Pd_1/γ-Al_2O_3 and Ag_1Pd_1/γ-Al_2O_3 hardly show any activity; however, the 1,3-butadiene conversion of Ag_1Pd_3/γ-Al_2O_3 is up to 100%, which reaches the same conversion as Pd/γ-Al_2O_3. Specially, the highest yield (84.9%) of butane was obtained by the Ag_1Pd_3/γ-Al_2O_3 bimetallic catalyst. It should be noted that the results in Table 1 reflect the integrated effects of particle size and composition on the catalytic performance because the tested catalysts were not provided with a uniform size (Figure 3). However, when comparing Ag_1Pd_3/γ-Al_2O_3 and Pd/γ-Al_2O_3 with the same metal loading (0.5 wt %) and similar size (7.4 and 7.3 nm, respectively), enhanced butene selectivity and yields by the bimetallic Ag−Pd catalysts can be evidently observed. The promotional effects of Ag−Pd alloy catalysts might be attributed to the synergetic effect of alloy in the hydrogenation, and the addition of Ag could suppress full hydrogenation and increase selectivity to butene.[46,47]

Figure 8 shows the time-on-stream plot of 1,3-butadiene conversion and butene selectivity over the Ag_1Pd_3/γ-Al_2O_3 catalyst at 35 °C versus the reaction time. No obvious loss in activity was observed, and the butene selectivity remained at constant levels within time-on-stream of 12 h, indicating that the the Ag_1Pd_3/γ-Al_2O_3 alloy catalyst also possesses desired stability in addition to excellent catalytic performance.

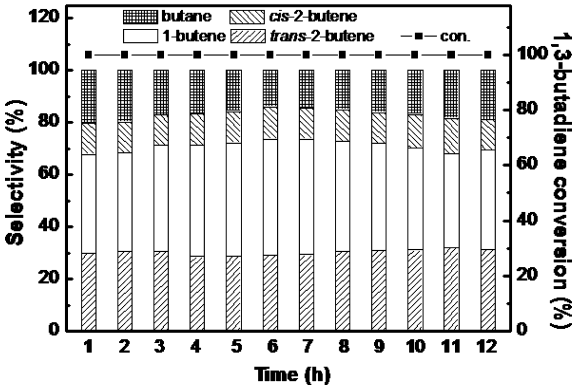

Figure 8. Time-on-stream plot of 1,3-butadiene conversion and butene selectivity over Ag_1Pd_3/γ-Al_2O_3.

CONCLUSIONS

In conclusion, Ag−Pd bimetallic alloy NPs have been successfully achieved by using *Cacumen platycladi* leaves extract, which acted as both the reducing agent and stabilizing agent. The alloy nature of the as-prepared NPs was confirmed by XRD, TEM, SAED, and EDX. The FTIR analysis indicated that biomolecules like saccharides, polyphenols, or carbonyl compounds were important in the reduction process, while biocomponds with (NH)C═O groups like proteins were responsible for the stabilization of the NPs. Such an approach to formation of alloy NPs was facile, hazard free, and environment friendly. Furthermore, Ag−Pd/γ-Al_2O_3-supported bimetallic catalysts were prepared out of the as-prepared Ag−Pd alloy NPs. Ag_1Pd_3/γ-Al_2O_3 demonstrated excellent catalytic performance toward selective hydrogenation of 1,3-butadiene with the highest butene yield of 84.9% at 35 °C, and it also presented desired stability within time-on-stream of 12 h.

Table 1. Catalytic Performance of Ag−Pd/γ-Al_2O_3 with different initial Ag/Pd ratios and Ag/γ-Al_2O_3 and Pd/γ-Al_2O_3 Catalysts for Selective Hydrogenation of 1,3-Butadiene[a]

		selectivity (%)				
sample	conversion (%)	1-butene	*cis*-2-butene	*trans*-2-butene	butane	yield (%)
Ag/γ-Al_2O_3	0	0	0	0	0	0
Ag_3Pd_1/γ-Al_2O_3	0.4	15.3	65.7	19.0	0	0.4
Ag_1Pd_1/γ-Al_2O_3	0.9	30.1	32.7	30.6	6.6	0.9
Ag_1Pd_3/γ-Al_2O_3	100	42.0	12.2	30.7	15.1	84.9
Pd/γ-Al_2O_3	100	7.0	11.3	32.9	48.8	51.2

[a]Metal loadings of all catalysts are 0.5 wt %.

AUTHOR INFORMATION

Corresponding Authors

*D. Sun: E-mail: sdaohua@xmu.edu.cn.

*Q. Li: E-mail: kelqb@xmu.edu.cn.

Notes

The authors declare no competing financial interest.

ACKNOWLEDGMENTS

The authors are thankful for the financial support of the NSFC projects (21036004), Natural Science Foundation of Fujian (2013J01059), and Science and Technology Program of Xiamen (3502Z20133006).

REFERENCES

(1) Zhan, G.; Hong, Y.; Mbah, V. T.; Huang, J.; Ibrahim, A. R.; Du, M.; Li, Q. Bimetallic Au−Pd/MgO as efficient catalysts for aerobic oxidation of benzyl alcohol: A green bio-reducing preparation method. *Appl. Catal., A* **2012**, *439*−*440*, 179−186.

(2) Kan, C.; Cai, W.; Li, C.; Zhang, L.; Hofmeister, H. Ultrasonic synthesis and optical properties of Au/Pd bimetallic nanoparticles in ethylene glycol. *J. Phys. D: Appl. Phys.* **2003**, *36*, 1609−1614.

(3) Schrick, B.; L, J.; Blough, A.; Jones, D.; Mallouk, T. E. Hydrodechlorination of trichloroethylene to hydrocarbons using bimetallic nickel-iron nanoparticles. *Chem. Mater.* **2002**, *14*, 5140−5147.

(4) Kim, K.; Kim, K. L.; Shin, K. S. Co-reduced Ag/Pd bimetallic nanoparticles: surface enrichment of Pd revealed by raman spectroscopy. *J. Phys. Chem. C* **2011**, *115*, 14844−14851.

(5) Jiang, Y.; Lu, Y.; Han, D.; Zhang, Q.; Niu, L. Hollow Ag@ Pd core−shell nanotubes as highly active catalysts for the electrooxidation of formic acid. *Nanotechnology* **2012**, *23*, 105609.

(6) Sandoval, A.; Aguilar, A.; Louis, C.; Traverse, A.; Zanella, R. Bimetallic Au−Ag/TiO_2 catalyst prepared by deposition−precipitation: High activity and stability in CO oxidation. *J. Catal.* **2011**, *281*, 40−49.

(7) Cheng, L. C.; Huang, J. H.; Chen, H. M.; Lai, T. C.; Yang, K. Y.; Liu, R. S.; Hsiao, M.; Chen, C. H.; Her, L. J.; Tsai, D. P. Seedless, silver-induced synthesis of star-shaped gold/silver bimetallic nanoparticles as high efficiency photothermal therapy reagent. *J. Mater. Chem.* **2012**, *22*, 2244−2253.

(8) Sankar, M.; Dimitratos, N.; Miedziak, P. J.; Wells, P. P.; Kiely, C. J.; Hutchings, G. J. Designing bimetallic catalysts for a green and sustainable future. *Chem. Soc. Rev.* **2012**, *41*, 8099−8139.

(9) Bönnemann, H.; Richards, R. M. Nanoscopic metal particles−synthetic methods and potential applications. *Eur. J. Inorg. Chem.* **2001**, *2001*, 2455−2480.

(10) Burda, C.; Chen, X.; Narayanan, R.; El-Sayed, M. A. Chemistry and properties of nanocrystals of different shapes. *Chem. Rev.* **2005**, *105*, 1025−1102.

(11) Bönnemann, H.; Nagabhushana, K. S. Metal Nanoclusters: Synthesis and Strategies for Their Size Control. In *Metal Nanoclusters in Catalysis and Materials Science. The Issue of Size Control*; Elsevier BV: Amsterdam, 2007, 21−48.

(12) Chou, N. H.; Schaak, R. E. Shape-controlled conversion of β-Sn nanocrystals into intermetallic M-Sn (M = Fe, Co, Ni, Pd) nanocrystals. *J. Am. Chem. Soc.* **2007**, *129*, 7339−7345.

(13) Wu, J.; Zhang, J.; Peng, Z.; Yang, S.; Wagner, F. T.; Yang, H. Truncated octahedral Pt_3Ni oxygen reduction reaction electrocatalysts. *J. Am. Chem. Soc.* **2010**, *132*, 4984−4985.

(14) Shankar, S. Rapid synthesis of Au, Ag, and bimetallic Au core−Ag shell nanoparticles using Neem (*Azadirachta indica*) leaf broth. *J. Colloid Interface Sci.* **2004**, *275*, 496−502.

(15) Gan, P. P.; Li, S. F. Y. Potential of plant as a biological factory to synthesize gold and silver nanoparticles and their applications. *Rev. Environ. Sci. Bio/Technol.* **2012**, *11*, 169−206.

(16) Sundaravadivelan, C.; Nalini Padmanabhan, M.; Sivaprasath, P.; Kishmu, L. Biosynthesized silver nanoparticles from *Pedilanthus tithymaloides* leaf extract with anti-developmental activity against larval instars of *Aedes aegypti* L. (Diptera; Culicidae). *Parasitology Research* **2013**, *112*, 303−11.

(17) Kotakadi, V. S.; Rao, Y. S.; Gaddam, S. A.; Prasad, T. N.; Reddy, A. V.; Gopal, D. V. Simple and rapid biosynthesis of stable silver nanoparticles using dried leaves of *Catharanthus roseus*. Linn. G. Donn and its anti microbial activity. *Colloids Surf., B* **2013**, *105*, 194−8.

(18) Vanaja, M.; Annadurai, G. *Coleus aromaticus* leaf extract mediated synthesis of silver nanoparticles and its bactericidal activity. *Appl. Nanosci.* **2012**, *3*, 217−223.

(19) Zargar, M.; Hamid, A. A.; Bakar, F. A.; Shamsudin, M. N.; Shameli, K.; Jahanshiri, F.; Farahani, F. Green synthesis and antibacterial effect of silver nanoparticles using *Vitex negundo L. Molecules* **2011**, *16*, 6667−6676.

(20) Gardea-Torresdey, J. L.; Gomez, E.; Peralta-Videa, J. R.; Parsons, J. G.; Troiani, H.; Jose-Yacaman, M. Alfalfa sprouts: A natural source for the synthesis of silver nanoparticles. *Langmuir* **2003**, *19*, 1357−1361.

(21) Yang, X.; Li, Q. B.; Wang, H. X.; Huang, J. L.; Lin, L. Q.; Wang, W. T.; Sun, D. H.; Su, Y. B.; Opiyo, J. B.; Hong, L. W.; Wang, Y. P.; He, N.; Jia, L. S. Green synthesis of palladium nanoparticles using broth of *Cinnamomum camphora* leaf. *J. Nanopart. Res.* **2010**, *12*, 1589−1598.

(22) Kanchana, A.; Devarajan, S.; Rathakrishnan Ayyappan, S. Green synthesis and characterization of palladium nanoparticles and its conjugates from *Solanum trilobatum* leaf extract. *Nano-Micro Lett.* **2010**, *2*, 169−176.

(23) Nadagouda, M. N.; Varma, R. S. Green synthesis of silver and palladium nanoparticles at room temperature using coffee and tea extract. *Green Chem.* **2008**, *10*, 859−862.

(24) Zhang, G.; Du, M.; Li, Q.; Li, X.; Huang, J.; Jiang, X.; Sun, D. Green synthesis of Au−Ag alloy nanoparticles using *Cacumen platycladi* extract. *RSC Adv.* **2013**, *3*, 1878.

(25) Sheny, D. S.; Mathew, J.; Philip, D. Phytosynthesis of Au, Ag and Au−Ag bimetallic nanoparticles using aqueous extract and dried leaf of *Anacardium occidentale*. *Spectrochim. Acta, Part A* **2011**, *79*, 254−262.

(26) Mondal, S.; Roy, N.; Laskar, R. A.; Sk, I.; Basu, S.; Mandal, D.; Begum, N. A. Biogenic synthesis of Ag, Au and bimetallic Au/Ag alloy nanoparticles using aqueous extract of mahogany (*Swietenia mahogani* JACQ.) leaves. *Colloid Surface B* **2011**, *82*, 497−504.

(27) Schabes-Retchkiman, P. S.; Canizal, G.; Herrera-Becerra, R.; Zorrilla, C.; Liu, H. B.; Ascencio, J. A. Biosynthesis and characterization of Ti/Ni bimetallic nanoparticles. *Opt. Mater.* **2006**, *29*, 95−99.

(28) Liu, H. B.; Canizal, G.; Schabes-Retchkiman, P. S.; Ascencio, J. A. Structural selection and amorphization of small Ni-Ti bimetallic clusters. *J. Phys. Chem. B* **2006**, *110*, 12333−12339.

(29) Liu, H.; Huang, J.; Sun, D.; Lin, L.; Lin, W.; Li, J.; Jiang, X.; Wu, W.; Li, Q. Microfluidic biosynthesis of silver nanoparticles: Effect of process parameters on size distribution. *Chem. Eng. J.* **2012**, *209*, 568−576.

(30) Lin, L.; Wang, W.; Huang, J.; Li, Q.; Sun, D.; Yang, X.; Wang, H.; He, N.; Wang, Y. Nature factory of silver nanowires: Plant-mediated synthesis using broth of *Cassia fistula* leaf. *Chem. Eng. J.* **2010**, *162*, 852−858.

(31) Jia, L. S.; Zhang, Q.; Li, Q. B.; Song, H. The biosynthesis of palladium nanoparticles by antioxidants in *Gardenia jasminoides Ellis*: Long lifetime nanocatalysts for p-nitrotoluene hydrogenation. *Nanotechnology* **2009**, *20*, 385601.

(32) Huang, J. L.; Li, Q. B.; Sun, D. H.; Lu, Y. H.; Su, Y. B.; Yang, X.; Wang, H. X.; Wang, Y. P.; Shao, W. Y.; He, N.; Hong, J. Q.; Chen, C. X. Biosynthesis of silver and gold nanoparticles by novel sundried *Cinnamomum camphora* leaf. *Nanotechnology* **2007**, *18*, 105104.

(33) Shankar, S. S.; Ahmad, A.; Pasricha, R.; Sastry, M. Bioreduction of chloroaurate ions by geranium leaves and its endophytic fungus yields gold nanoparticles of different shapes. *J. Mater. Chem.* **2003**, *13*, 1822−1826.

(34) Shankar, S. S.; Rai, A.; Ankamwar, B.; Singh, A.; Ahmad, A.; Sastry, M. Biological synthesis of triangular gold nanoprisms. *Nat. Mater.* **2004**, *3*, 482−488.
(35) Liu, H.; Wang, D.; Shang, S.; Song, Z. Synthesis and characterization of Ag−Pd alloy nanoparticles/carboxylated cellulose nanocrystals nanocomposites. *Carbohydr. Polym.* **2011**, *83*, 38−43.
(36) Ferrando, R.; Jellinek, J.; Johnston, R. L. Nanoalloys: From theory to applications of alloy clusters and nanoparticles. *Chem. Rev.* **2008**, *108*, 845−910.
(37) Toshima, N.; Yonezawa, T. Bimetallic nanoparticles−novel materials for chemical and physical applications. *New J. Chem.* **1998**, *22*, 1179−1201.
(38) Zhan, G.; Huang, J.; Du, M.; Abdul-Rauf, I.; Ma, Y.; Li, Q. Green synthesis of Au−Pd bimetallic nanoparticles: Single-step bioreduction method with plant extract. *Mater. Lett.* **2011**, *65*, 2989−2991.
(39) Chen, D. H.; Chen, C. J. Formation and characterization of Au−Ag bimetallic nanoparticles in water-in-oil microemulsions. *J. Mater. Chem.* **2002**, *12*, 1557−1562.
(40) Ji, Y.; Yang, S.; Guo, S.; Song, X.; Ding, B.; Yang, Z. Bimetallic Ag/Au nanoparticles: A low temperature ripening strategy in aqueous solution. *Colloids Surf., A* **2010**, *372*, 204−209.
(41) Nemamcha, A.; Rehspringer, J. L.; Khatmi, D. Synthesis of palladium nanoparticles by sonochemical reduction of palladium(II) nitrate in aqueous solution. *J. Phys. Chem. B* **2006**, *110*, 383−387.
(42) Hub, S.; Hilaire, L.; Touroude, R. Hydrogenation of but-1-yne and but-1-ene on palladium catalysts: particle size effect. *Appl. Catal.* **1988**, *36*, 307−322.
(43) Pattamakomsan, K.; Ehret, E.; Morfin, F.; Gélin, P.; Jugnet, Y.; Prakash, S.; Bertolini, J. C.; Panpranot, J.; Aires, F. J. C. S. Selective hydrogenation of 1,3-butadiene over Pd and Pd−Sn catalysts supported on different phases of alumina. *Catal. Today* **2011**, *164*, 28−33.
(44) Goetz, J. Low-loaded Pd−Pb/α-Al_2O_3 catalysts: Effect of alloying in the hydrogenation of buta-1,3-diene and hydrogenation and isomerization of butenes. *J. Catal.* **2001**, *199*, 338−345.
(45) Garron, A.; Lázár, K.; Epron, F. Effect of the support on tin distribution in Pd−Sn/Al_2O_3 and Pd−Sn/SiO_2 catalysts for application in water denitration. *Appl. Catal., B* **2005**, *59*, 57−69.
(46) Gonzalez, S.; Neyman, K. M.; Shaikhutdinov, S.; Freund, H.-J.; Illas, F. On the promoting role of Ag in selective hydrogenation reactions over Pd−Ag bimetallic catalysts: A theoretical study. *J. Phys. Chem. C* **2007**, *111*, 6852−6856.
(47) Zhang, Q.; Li, J.; Liu, X.; Zhu, Q. Synergetic effect of Pd and Ag dispersed on Al_2O_3 in the selective hydrogenation of acetylene. *Appl. Catal., A* **2000**, *197*, 221−228.